CHEMISTRY OF MATERIALS

ARTICLE

pubs.acs.org/cm

Investigation of the Effects of Polyhedral Gold Nanocrystal Morphology and Facets on the Formation of Au−Cu_2O Core−Shell Heterostructures

Wei-Ching Wang, Lian-Ming Lyu, and Michael H. Huang*

Department of Chemistry, National Tsing Hua University, Hsinchu 30013, Taiwan

Supporting Information

ABSTRACT: Rhombic dodecahedral and highly edge- and corner-truncated octahedral gold nanocrystal cores with entirely or significant {110} faces were employed to investigate the core−shell orientation relationship of Au−Cu_2O core−shell heterostructures. By increasing the volume of reductant added, we synthesized Au−Cu_2O face-raised cubes, cuboctahedra, and octahedra. TEM characterization indicates a fixed core−shell orientation relationship. The {100}, {110}, and {111} facets of the gold cores align parallel to the corresponding faces of the Cu_2O shells. Structural requirements of the gold cores for the preparation of Au−Cu_2O stellated icosahedra indicate that icosahedral gold nanocrystals are good candidates. Use of trisoctahedral nanocrystal cores cannot generate stellated icosahedra, but unusual face-raised octahedra with V-shaped {111} edges can be synthesized. Core−shell cubes, face-raised cubes, core−shell octahedra, and face-raised octahedra were examined for their comparative photocatalytic activity toward the photodegradation of methyl orange. Remarkably, all the cubes were found to be photocatalytically inactive because they are bounded by essentially {100} facets. Face-raised octahedra with more {111} facets showed significantly better photocatalytic performance than regular Au−Cu_2O core−shell octahedra. The results reveal that gold nanocrystal-enhanced photocatalysis can be achieved only with Cu_2O shells exposing proper facets.

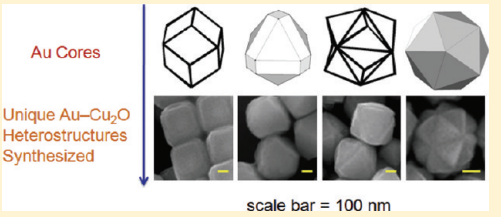

KEYWORDS: core−shell heterostructures, cuprous oxide, gold, nanostructures, photocatalysis

INTRODUCTION

Nanoscale core−shell heterostructures are an important class of nanostructures for both fundamental science and real applications such as in biomedical applications, magnetic separation, and enhanced photoluminescence.[1−3] They may also be used to fabricate hollow nanostructures.[4] Many kinds of core−shell heterostructures have been synthesized. It is relatively easy to make core−shell nanocrystals without morphology control of both the cores and the shells. However, a recent and more challenging attempt is to prepare core−shell heterostructures using polyhedral metal nanocrystal cores to direct the growth of shells with excellent control of shell morphologies.[5−11] Bimetallic core−shell systems have been examined in these studies. The new heterostructures may show enhanced electrocatalytic activity.[6,9,11]

We have previously reported the synthesis of Cu_2O nanocrystals with systematic shape evolution from cubic to cuboctahedral and octahedral structures in aqueous solution at room temperature.[12−14] Truncated rhombic dodecahedral Cu_2O nanocages and nanoframes can be formed using the condition for synthesizing cuboctahedral Cu_2O nanocrystals by adding HCl.[15] Octahedral gold nanocrystals and long gold nanorods can be easily trapped inside the nanocages and nanoframes. On the basis of these studies, different gold nanostructures including octahedral nanocrystals, highly faceted nanocrystals, long nanorods, and nanoplates have been used as cores for the fabrication of Au−Cu_2O core−shell heterostructures with precise control of shell morphologies by using the same synthetic method but without the addition of HCl.[16] These heterostructures represent the first example of metal−semiconductor core−shell systems with morphological control of both components. When octahedral gold nanocrystal cores were used, the Cu_2O shell morphology can still be tuned from cubic to octahedral structures by varying the volume of $NH_2OH·HCl$ reductant added. The heterostructures exhibit highly facet-dependent and Au nanocrystal-enhanced electrical and photocatalytic properties, demonstrating the importance of shell morphology control and the gold cores.[17] Cubic and octahedral Au−Cu_2O core−shell heterostructures can also convert into Cu_2S nanocages of the corresponding morphologies with encapsulated Au nanocrystals.[18] The gold core has an exact orientation relationship with the Cu_2O shell. All corners of the octahedral gold core are directed perpendicular to the {100} faces of the Cu_2O shell, and all faces of the octahedral gold core are parallel to the {111} facets of the Cu_2O shell. However, it is not clear if gold nanocrystals with significant or only {110} surfaces can form core−shell heterostructures with systematic shape evolution. The core−shell orientation relationship also needs to be analyzed. In this study, we have used rhombic dodecahedral and edge- and corner-truncated gold nanocrystals as structure-directing cores for the fabrication of Au−Cu_2O core−shell heterostructures with

Received: March 10, 2011
Revised: April 14, 2011
Published: April 27, 2011

dx.doi.org/10.1021/cm200708q | *Chem. Mater.* 2011, 23, 2677–2684

systematic shape evolution. The cores contain only or significant {110} surface facets. The heterostructures have been carefully examined to establish the orientation relationship between the cores and the shells.

Another important result from our investigation on the growth of Au−Cu_2O core−shell heterostructures is the formation of novel stellated icosahedra using highly faceted gold nanocrystal cores.[16] Yet these gold cores are not so structurally well-defined and uniform. It is interesting to consider which polyhedral geometry may serve as effective cores for the overgrowth of Cu_2O with a stellated icosahedral morphology. Here we show that icosahedral gold nanocrystals are effective cores. Interestingly, trisoctahedral gold nanocrystals possessing {221} facets cannot produce stellated icosahedra, but they form unusual face-raised octahedral heterostructures. Some of the new cubic and octahedral heterostructures have not been tested for their comparative photocatalytic activity. Photocatalytic experiments have been carried out using these nanocrystals. The results offer additional insights to our understanding of the facet-dependent photocatalytic properties of Cu_2O crystals.

EXPERIMENTAL SECTION

The gold nanocrystal cores used in this study were synthesized following the procedures developed in our laboratory. The methods used for the preparation of rhombic dodecahedral and trisoctahedral Au nanocrystals follow the seed-mediated procedure described earlier.[19] The reagents were obtained from the same manufacturers as before. Briefly, freshly made gold seed particles were added to a growth solution of cetyltrimethylammonium chloride (CTAC) surfactant, $HAuCl_4$, ascorbic acid, NaBr, and water. After being stirred for a few seconds, a small amount of this growth solution was transferred to another growth solution for nanocrystal growth at 30 °C for 15 min. By replacing NaBr with KI and adjusting the amount of ascorbic acid added, edge- and corner-truncated octahedral gold nanocrystals can be obtained. For the formation of icosahedral gold nanocrystals, the procedure described to make penta-branched gold nanocrystals but without the addition of $AgNO_3$ was slightly modified.[20] Details of the experimental procedures for the syntheses of these gold nanocrystals are available in the Supporting Information. All Au nanocrystal cores were finally dispersed in 1 mL of deionized water.

The fabrication of Au−Cu_2O core−shell heterostructures follows our previously reported procedure.[16] In a typical synthesis of the Au−Cu_2O core−shell heterostructures, 4.725, 4.65, or 4.45 mL of deionized water (for cubic, cuboctahedral, or octahedral Cu_2O shell morphology, respectively), 0.1 mL of 1×10^{-3} M $CuCl_2$ solution, 0.0435 g of sodium dodecyl sulfate (SDS), 50 μL of the Au nanocrystal core solution, and 125 μL of 1.0 M NaOH were introduced into a sample vial in the order listed. Then 75, 175, or 325 μL of 0.2 M $NH_2OH \cdot HCl$ was added to obtain Cu_2O shells with cubic, cuboctahedral, or octahedral morphology, respectively. The total solution volume is 5 mL. Scheme S1 in the Supporting Information summarizes the procedure used. After the addition of $NH_2OH \cdot HCl$, the solution color turned from purple to yellow and finally light brown after keeping the mixture undisturbed for 2 h. To collect the products, all solutions were washed with deionized water and centrifuged four times at 3000 rpm for 5 min to remove the surfactant. The precipitate was dispersed in 0.5 mL of ethanol.

For photocatalytic activity measurements, the amount of Au−Cu_2O core−shell heterostructures needed is much more than can be generated from the above procedure. Thus, we used 20 times more reagent amounts to synthesize the Au−Cu_2O core−shell nanocrystal samples here, such that the total solution volume is 100 mL. The entire centrifuged Au−Cu_2O core−shell nanocrystals were dispersed in 90 mL of 15 mg/L aqueous methyl orange solution. The entire solution was transferred to a homemade cubic quartz cell with an inner cell edge length of about 4.5 cm and a small capped opening at the top. Before illumination, the cell was constantly stirred for 30 min in the dark for the dye molecules to complete adsorb on the Cu_2O surface. After that the cell was irradiated with light from a 500 W xenon lamp. The lamp was placed 28 cm away from the center of the cell. The light intensity reaching the cell was measured to be 245 mW/cm^2 using a power meter. UV−vis absorption spectra of these samples were taken before and after every 60 min of irradiation for up to 240 min by removing the cap to withdraw the solution.

Scanning electron microscopy (SEM) images of the samples were obtained using a JEOL JSM-7000F electron microscope. Transmission electron microscopy (TEM) characterization was performed on JEOL JEM-2010 and JEM-2100 electron microscopes with an operating voltage of 200 kV. High-resolution transmission electron microscopy (HR-TEM) characterization was performed on a JEOL JEM-3000F electron microscope with an operating voltage of 300 kV. Powder X-ray diffraction (XRD) patterns were recorded on a Shimadzu XRD-6000 diffractometer with Cu Kα radiation (λ = 1.5418 Å). UV−vis absorption spectra were taken using a JASCO V-570 spectrophotometer.

RESULTS AND DISCUSSION

Cuprous oxide (Cu_2O) is a *p*-type semiconductor with a direct band gap of 2.17 eV.[21] Cu_2O has a cuprite crystal structure (a body-centered cubic packing of oxygen atoms with copper atoms occupying one-half of the tetrahedral sites). Its unit-cell parameter is 4.267 Å. Gold has a unit cell parameter of 4.0786 Å. In this study, we have examined the fabrication of Au−Cu_2O core−shell heterostructures with systematic evolution of shell morphology using gold nanocrystal cores possessing entirely or significant {110} surface facets. Rhombic dodecahedral and highly edge- and corner-truncated octahedral gold nanocrystals were used as the structure-directing cores. Rhombic dodecahedral gold nanocrystals bounded exclusively by {110} surfaces were synthesized following our reported procedure.[19] Edge- and corner-truncated octahedral nanocrystals contain significant {110} faces from the truncated edges. They were prepared by using similar synthetic conditions to those employed to make the rhombic dodecahedral gold nanocrystals but replacing NaBr with KI. Figure 1 presents SEM images of the synthesized rhombic dodecahedral gold nanocrystals and the resulting Au−Cu_2O core−shell heterostructures using these cores. Average particle size of the rhombic dodecahedra is around 90 nm. By adjusting the volume of $NH_2OH \cdot HCl$ reductant added from 75 to 175 and 325 μL, Au−Cu_2O core−shell heterostructures with cubic, cuboctahedral, and octahedral structures were obtained, respectively. Interestingly, the cubes appear to be slightly face-raised. Corner-truncated octahedra and short hexapods can also be prepared by adding 225 and 525 μL of $NH_2OH \cdot HCl$ (data not shown). Thus, systematic shape evolution of shell morphology can still be achieved here. The face-raised cubes, cuboctahedra, and octahedra have average sizes of 304, 345, and 373 nm. They are monodisperse in size with a standard deviation of 8% or less (see the Supporting Information Table S1 and size distribution histogram Figure S1). Formation of the Au−Cu_2O core−shell heterostructures using polyhedral gold cores has been shown to follow an unusual hollow shell-refilled (HSR) mechanism, in which the Cu_2O shells with a precise outer morphology are formed first via Cu_2O linkages to the cores before filling the spaces between the shells and the cores.[16] Systematic shape evolution of the Cu_2O shell is achieved through fine adjustment

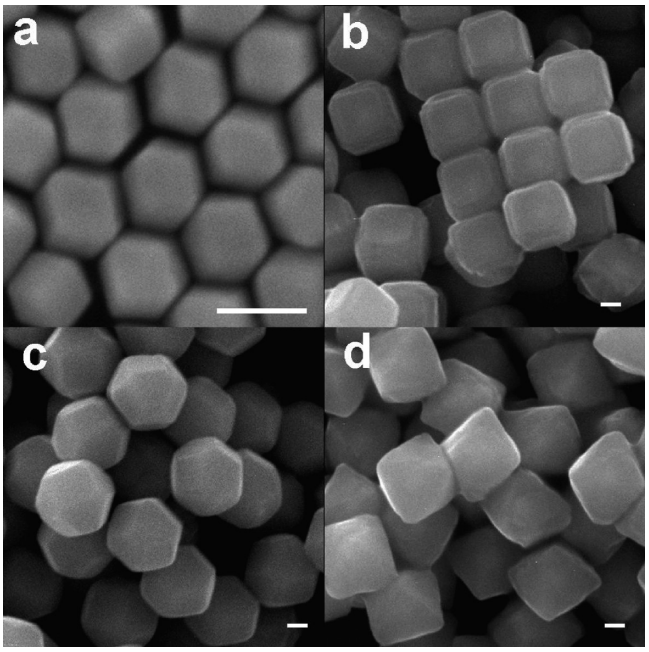

Figure 1. (a) SEM image of the synthesized rhombic dodecahedral gold nanocrystals. (b−d) SEM images of the Au−Cu_2O core−shell nanocrystals synthesized using rhombic dodecahedral gold nanocrystal cores. By varying the volume of $NH_2OH \cdot HCl$ added, (b) face-raised cubes, (c) cuboctahedra, and (d) octahedra were obtained. All scale bars are equal to 100 nm.

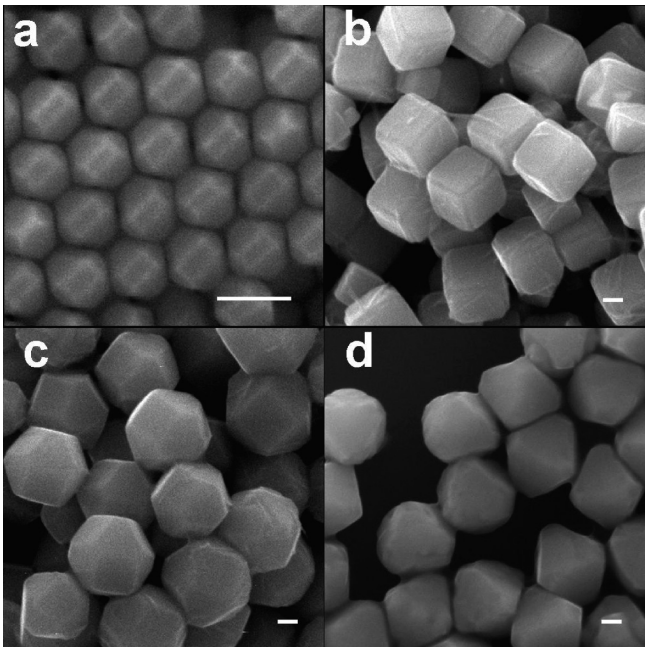

Figure 2. (a) SEM image of the synthesized edge- and corner-truncated octahedral gold nanocrystals. (b−d) SEM images of the Au−Cu_2O core−shell nanocrystals synthesized using edge- and corner-truncated gold nanocrystal cores. By varying the volume of $NH_2OH \cdot HCl$ added, (b) face-raised cubes, (c) cuboctahedra, and (d) truncated octahedra were obtained. All scale bars are equal to 100 nm. The fibrous structures seen in panel (b) are likely $Cu(OH)_2$.

of the $NH_2OH \cdot HCl$ reductant volume and thus fine control of the reduction rate to form Cu_2O from $Cu(OH)_2$.[12,13]

Figure 2 shows SEM images of the synthesized edge- and corner-truncated octahedral gold nanocrystals and the resulting Au−Cu_2O core−shell heterostructures using these cores. Because of their shape uniformity, edge- and corner-truncated octahedral gold nanocrystals spontaneously self-assemble into an ordered packing structure with their {110} edges lying on the substrate surface. They have an average size of around 85 nm. By increasing the volume of reductant introduced, the Au−Cu_2O core−shell heterostructures evolve from face-raised cubic to cuboctahedral and truncated octahedral structures with respective average sizes of 283, 331, and 363 nm (see the Supporting Information, Table S2, and size distribution histogram, Figure S2).

For further characterization of the heterostructures, we carried out XRD and optical measurements. As expected, XRD patterns of all these samples show strong reflection peaks from Cu_2O and weak peaks from Au (see Figures S3 and S4 in the Supporting Information). Because of their preferential orientation of deposition on substrates, face-raised cubes show strong (200) reflection peak of Cu_2O. Octahedra and truncated octahedra exhibit strong (111) peak of Cu_2O. For cuboctahedra, the (111) peak is stronger than the (200) peak but their intensities are more comparable. UV−vis absorption spectrum of the rhombic dodecahedral gold nanocrystals gives a single absorption band centered at 565 nm, whereas the edge- and corner-truncated octahedral nanocrystals show a band centered at 560 nm. All six samples of the Au−Cu_2O core−shell heterostructures show similar spectral features (see Figures S5 and S6 in the Supporting Information). An absorption band is observed in the range of 455−475 nm, which blue-shifts slightly with increasing sizes of the heterostructures. The spectra are dominated by strong multiple light scattering bands due to their relatively large sizes of 280−370 nm. Two major bands are clearly identifiable at 595−615 and 710−740 nm. These bands are red-shifted progressively with decreasing particle sizes.

The orientation relationship between the cores and the shells in these heterostructures was extensively investigated using TEM, cross-sectional TEM, HR-TEM, and selected-electron diffraction (SAED) techniques. Figure 3 displays results of TEM characterization of a single Au−Cu_2O core−shell face-raised cube and octahedron synthesized using rhombic dodecahedral gold cores. To examine the interfacial epitaxial growth of the core−shell heterostructures and obtain better SAED patterns, the particles were sectioned by an ultramicrotome to reveal their cross-sectional views. The SEM images are provided to show the exact viewing directions of the respective TEM images and SAED patterns. TEM images of a face-raised cube viewed along the [111] direction and an octahedron viewed along the [110] direction are shown. The corresponding SAED patterns of the particles did not give sufficiently bright diffraction spots due to the thick Cu_2O shell (see panels a2 and b2). Significantly better SAED patterns were collected from the cross-sectional TEM samples that the diffraction spots from the gold cores can be seen (see panels a5 and b5). The projections of the inside cores are a hexagon and an elongated hexagon when viewed along the [111] and [110] directions (see panels a4 and b4). Drawings corresponding to the cross-sectional TEM images are also shown in panels a6 and b6. Some diffraction spots seen in panels a5 and b5 are contributed by the gold core. The (202) diffraction spot of Cu_2O and the (202) spot of Au are along the same direction (see panel a5). Both the cross-sectional TEM

dx.doi.org/10.1021/cm200708q |*Chem. Mater.* 2011, 23, 2677–2684

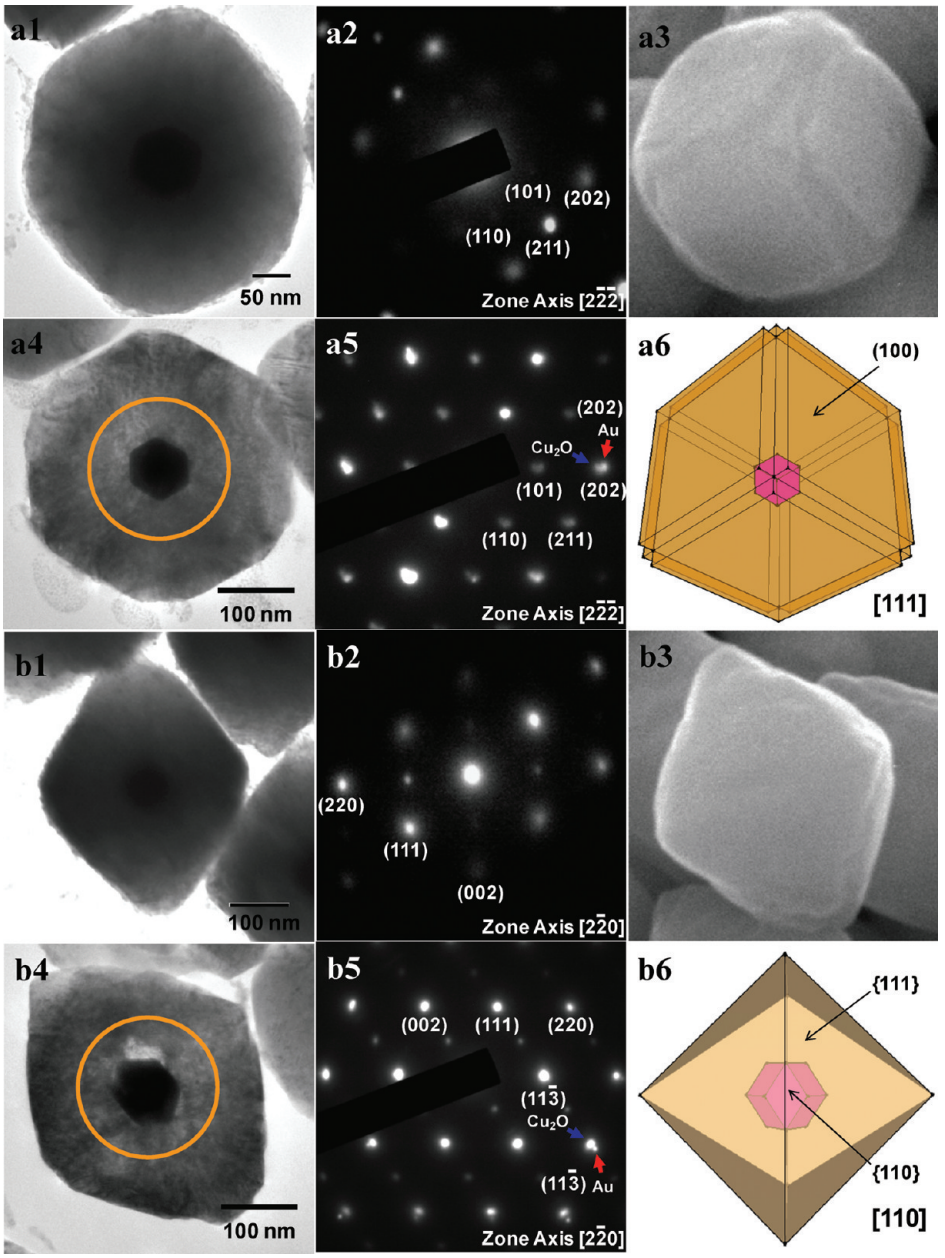

Figure 3. TEM Characterization of a single Au−Cu_2O core−shell face-raised cube and octahedron. Rhombic dodecahedral gold nanocrystal cores were used. (a1, b1) TEM images of the heterostructures viewed along the [111] and [110] directions. (a2, b2) SAED patterns corresponding to the TEM images. (a3, b3) SEM images of the heterostructures viewed along the [111] and [110] directions. (a4, b4) Cross-sectional TEM images of the heterostructures viewed along the [111] and [110] directions. (a5, b5) SAED patterns of the circled regions in panels a4 and b4. (a6, b6) Drawings showing the same particle orientation as the TEM images.

images and their corresponding SAED patterns reveal that the gold nanocrystal core has a fixed orientation relationship with the Cu_2O shell. The {110} facets of the rhombic dodecahedral core are exactly parallel to the {110} faces of Cu_2O. Thus, it is established that the [100], [110], and [111] directions of Au in the Au−Cu_2O core−shell heterostructures exactly matches the corresponding directions of Cu_2O. The reason that such an exact orientation relationship can be achieved is possibly because lattice mismatches of the corresponding (100) and (111) planes of Au and Cu_2O are acceptable for good epitaxial growth, such that the (200) planes of Cu_2O grow epitaxially over the {100} facet of the Au nanocrystal core, and that the (111) planes of Cu_2O grow over the {111} facet of Au (see HR-TEM images in Figure 4). The interfacial lattice mismatch between the (111) planes of Au and that of Cu_2O is 4.3%.[16] Once such parallel lattice growth is established, the orientation relationship is achieved as the shell forms via the HSR mechanism.[16] Interfacial lattice mismatch between the (110) planes of Au and Cu_2O is relatively poor at 7.9% (Au−Au roll-to-roll distance on the {110} facet is 3.929 Å, whereas the Cu−Cu or O−O distance on the {110} facet is 4.267 Å.) Thus, interfacial epitaxial growth may start from Cu_2O overgrowth on the {100} and {111} facets of Au.

The same core−shell orientation relationship analysis and the interfacial lattice growth situation was examined for single

dx.doi.org/10.1021/cm200708q |*Chem. Mater.* 2011, 23, 2677–2684

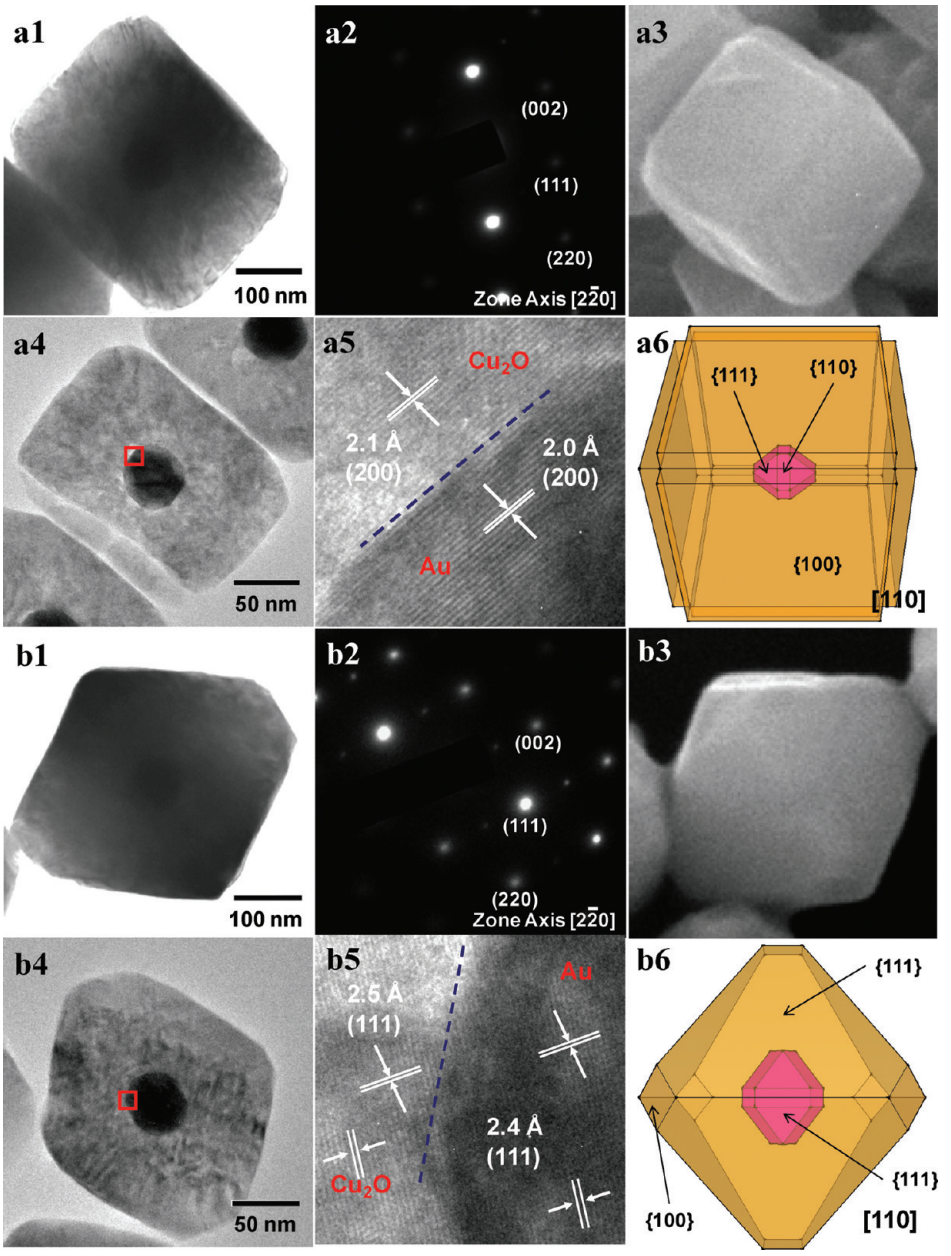

Figure 4. TEM Characterization of a single Au−Cu_2O core−shell face-raised cube and truncated octahedron. Edge- and corner-truncated octahedral gold nanocrystal cores were used. (a1, b1) TEM images of the heterostructures viewed along the [110] direction. (a2, b2) SAED patterns corresponding to the TEM images. (a3, b3) SEM images of the heterostructures viewed along the [110] direction. (a4, b4) Cross-sectional TEM images of the heterostructures viewed along the [110] direction. (a5, b5) Interfacial HR-TEM images of the red square regions in panels a4 and b4. (a6, b6) Drawings showing the same particle orientation as the TEM images.

Au−Cu_2O face-raised cubes and truncated octahedra synthesized using edge- and corner-truncated octahedral gold nanocrystal cores. Figure 4 gives the results of the TEM characterization. SEM images and drawings corresponding to the orientation of the particles seen in the TEM images are also provided. Both heterostructures were imaged along the [110] direction. TEM image of a face-raised cube viewed along the [100] direction is shown in Figure S7 in the Supporting Information. Complete cross-sectional TEM images of the particles shown in Figures 3 and 4 with viewing directions along the [100], [110], and [111] directions are available in Figure S8 in the Supporting Information. The core orientation with respect to the shell can be seen from the TEM images (panel b4 and arrow in panel a4). The SAED pattern of a cross-sectional truncated octahedron sample shows some diffraction spots from the gold core (see Figure S9 in the Supporting Information). The (220) diffraction spot of the gold core is at the same position as the (220) spot of Cu_2O, confirming their fixed orientation relationship. Interfacial HR-TEM images further indicate that the (200) planes of Cu_2O grow epitaxially on the (200) planes of Au, and that the (111) planes of Au are aligned in the same directions as the (111) planes of Cu_2O.

Another interesting aspect of this work is the investigation of structural requirements of polyhedral gold nanocrystals as cores

dx.doi.org/10.1021/cm200708q |*Chem. Mater.* 2011, 23, 2677–2684

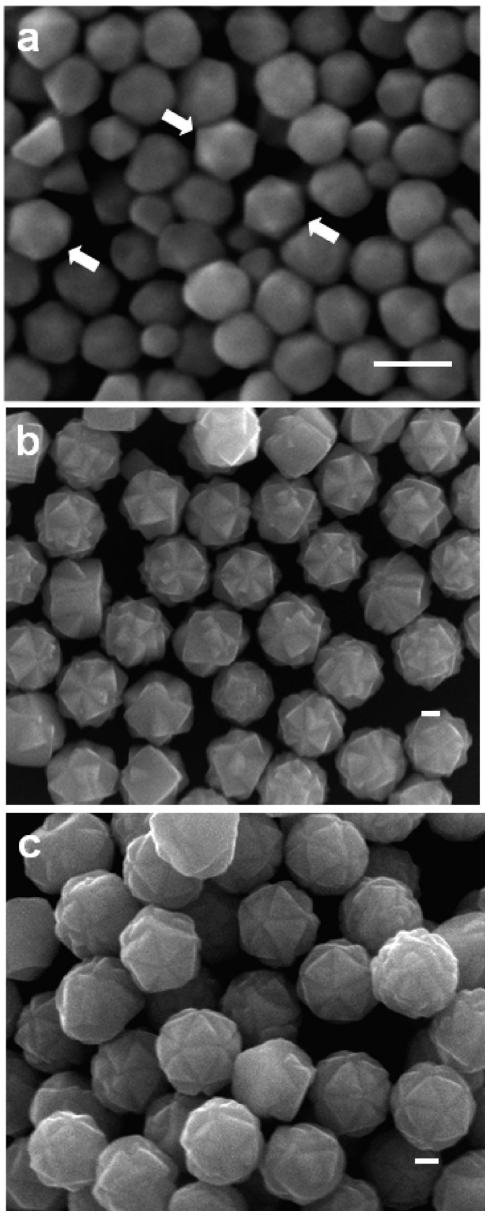

Figure 5. (a) SEM image of the icosahedral gold nanocrystals synthesized. Arrows indicate some perfect icosahedra. (b, c) SEM images of the Au−Cu_2O core−shell heterostructures with (b) stellated icosahedral and (c) truncated stellated icosahedral morphologies synthesized using the icosahedral Au nanocrystal cores. All scale bars are equal to 100 nm.

for the formation of unusual Au−Cu_2O core−shell stellated icosahedra. This study shows that rhombic dodecahedral and truncated octahedral gold nanocrystals cannot be used as cores for the generation of Au−Cu_2O stellated icosahedra, despite their possession of many surface facets. Gold nanocrystals with an icosahedral shape should naturally be a good candidate. We have adopted our seed-mediated procedure to make icosahedral gold nanocrystals.[20] Many icosahedral gold nanocrystals have been synthesized, although some particles are still not quite perfect in shape (see Figure 5a). Remarkably, Au−Cu_2O core−shell stellated icosahedra were synthesized using these cores (see Figure 5b). By increasing the volume of 0.2 M $NH_2OH·HCl$ from 0.15 to 0.25 mL, stellated icosahedra can also become truncated stellated icosahedra as observed in our previous report

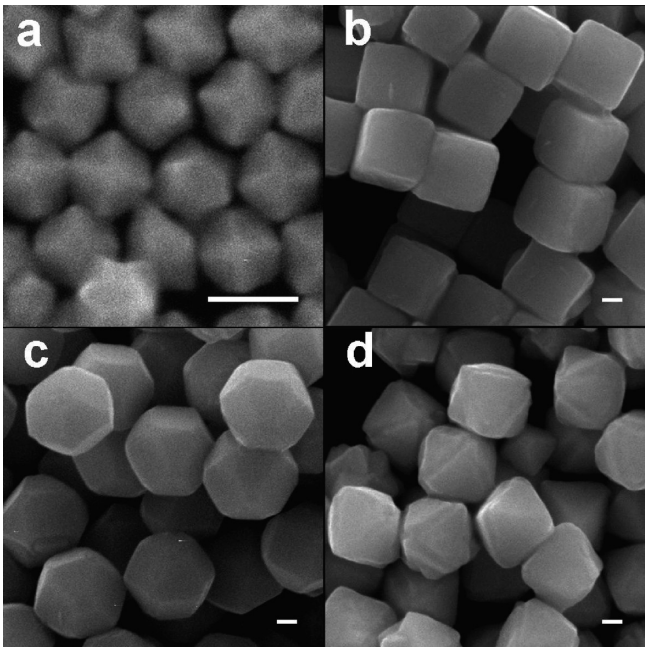

Figure 6. (a) SEM image of the synthesized trisoctahedral gold nanocrystals. (b−d) SEM images of the Au−Cu_2O core−shell nanocrystals synthesized using trisoctahedral gold nanocrystal cores. By varying the volume of $NH_2OH·HCl$ added, (b) cubes, (c) cuboctahedra, and (d) face-raised octahedra were obtained. All scale bars are equal to 100 nm.

(see Figure 5c).[16] Each stellated icosahedron is consisted of twenty triangular pyramids bounded by three {100} side faces and an {111} top face. Sharp tips are removed in a truncated stellated icosahedron to expose a larger fraction of {111} faces. Thus, icosahedral gold nanocrystals can serve as effective cores for the fabrication of Au−Cu_2O core−shell stellated icosahedra.

We have also examined the possibility of using trisoctahedral gold nanocrystals as cores for the formation of stellated icosahedra, as they possess 24 {221} facets. The trisoctahedral gold nanocrystals have sizes of around 90 nm (Figure 6a). By varying the volume of $NH_2OH·HCl$ added from 75 to 175 and 325 μL, we obtained Au−Cu_2O core−shell cubes, cuboctahedra, and face-raised octahedra (see Figure 6). They have sizes of mostly 340−380 nm (see Table S3 in the Supporting Information). Their XRD patterns look similar to the Au−Cu_2O core−shell heterostructures synthesized using the rhombic dodecahedral and edge- and corner-truncated gold cores (see Figure S10 in the Supporting Information). The face-raised octahedra are produced only with the use of trisoctahedral gold cores, so they also represent a new Au−Cu_2O heterostructure synthesized. Their V-shaped edges are likely consisted of {111} faces, as these faces are parallel to the {111} facets of the octahedra (see Figure S11 in the Supporting Information). The gold cores also maintain the same fixed orientation relationship with the Cu_2O shells. The results show that multifaceted trisoctahedral gold cores cannot be used to generate stellated icosahedra.

It is interesting to compare the relative photocatalytic activity of the face-raised cubes and octahedra to the normal Au−Cu_2O core−shell cubes and octahedra. New insights have been found. Previously we have demonstrated that pristine Cu_2O octahedra are photocatalytically active in the photodegradation of methyl orange, while sharp-faced Cu_2O cubes are inactive.[13] Cu_2O

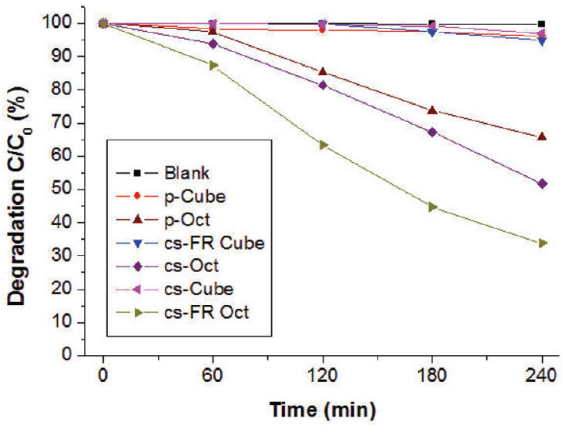

Figure 7. Plot of the extent of photodegradation of methyl orange vs time using various pristine Cu_2O nanocrystals and Au−Cu_2O core−shell heterostructures. Pristine cubes and octahedra (p-Cube and p-Oct) were synthesized following our previously reported procedure.[13] For the core−shell face-raised cubes and core−shell octahedra (cs-FR Cube and cs-Oct), rhombic dodecahedral Au nanocrystal cores were used. For the core−shell cubes and core−shell face-raised octahedra (cs-Cube and cs-FR Oct), trisoctahedral Au nanocrystal cores were employed.

crystals bounded by {111} faces contain terminal copper atoms and the surfaces are expected to be more positively charged, whereas those bound by the {100} faces such as cubes are electrically neutral or less charged. Octahedral Cu_2O crystals retaining positive charges on the surface will interact more strongly with negatively charged molecules and photodegradation of these molecules is more effective. Au−Cu_2O core−shell cubes and octahedra have been found to display an enhanced photocatalytic activity due to the presence of the gold cores, which efficiently separate photogenerated electrons and holes.[17] Figure 7 gives a plot of the extent of photodegradation of methyl orange vs time using various pristine Cu_2O nanocrystals and Au−Cu_2O core−shell heterostructures. The amount of nanocrystals added in each sample is twice that used in our previous photocatalysis investigation with Au−Cu_2O heterostructures, whereas the volume of the methyl orange solution used is the same as before.[17] Although the catalyst particle concentration is two times higher than before, the photodegradation rate and thus the extent of methyl orange degradation for pristine Cu_2O and core−shell octahedra is fairly consistent with results obtained previously. Core−shell face-raised cubes and core−shell octahedra were synthesized using rhombic dodecahedral gold cores. Core−shell cubes and face-raised octahedra were prepared with the use of trisocathedral gold cores. After irradiation for 4 h, the fraction of remaining absorbance of methyl orange measured at 462 nm was 99.7% for the blank sample, 96.2% for Cu_2O cubes, 65.6% for Cu_2O octahedra, 97.0% for core−shell cubes, 94.9% for core−shell face-raised cubes, 51.7% for core−shell octahedra, and 33.8% for core−shell face-raised octahedra (see Figure S12 in the Supporting Information for the UV−vis spectra). The results for the core−shell octahedra and pristine cubes and octahedra are expected. Surprisingly, the core−shell cubes and face-raised cubes are practically inactive toward photodegradation, despite the presence of gold nanocrystal cores. A close examination suggests that the results are not in conflict with our previous observation. The core−shell cubes and face-raised cubes synthesized in this study are bounded by essentially {100} facets, whereas core−shell cubes analyzed previously contain truncated {110} edges and {111} corners.[17] The {110} facets of Cu_2O has been shown to be more photocatalytically active than the {111} facets due to their higher surface energy and greater density of copper dangling bonds.[22] A new insight this study provides is that surface facets of Cu_2O is most important to its photocatalysis performance. Gold nanocrystal cores cannot enhance the photocatalytic activity of Au−Cu_2O core−shell heterostructures exposing only or mostly {100} facets. On the other hand, core−shell face-raised octahedra are the best photocatalysts. They have similar sizes to those of the core−shell octahedra (378 nm vs 373 nm, see the Supporting Information), so their total surface areas should be similar. It is presumed that the presence of additional V-shaped {111} edges and the gold core enhances the overall catalytic activity. Extended Cu_2O hexapods with 24 {111} facets also show a greatly enhanced photocatalytic activity when compared to that of Cu_2O octahedra.[13] Finally, all four core−shell heterostructures after performing photocatalysis for 4 h were inspected for their morphologies (see Figure S12 in the Supporting Information). Core−shell cubes and face-raised cubes maintained their shapes. Core−shell octahedra show etched corners as previously observed, suggesting the corners as active sites for photocatalysis.[17] Face-raised octahedra also display etched corners, but some particles have slightly etched faces. This situation affects the extended use of the photocatalysts. The core−shell octahedra have been used for the same photocatalytic experiment three times. The photocatalysts worked but showed gradually decreasing activity.

CONCLUSIONS

In this study, rhombic dodecahedral and edge- and corner-truncated octahedral gold nanocrystals with entirely or significant {110} facets have been used as structure-directing cores for the fabrication of Au−Cu_2O core−shell heterostructures. By varying the volume of reductant added, shell morphology can be systematically tuned from face-raised cubic to cuboctahedral and octahedral structures. Extensive TEM analysis confirms that these gold cores have an exact orientation relationship with the Cu_2O shells. The {100}, {110}, and {111} faces of the gold nanocrystal cores are parallel to the corresponding faces of the Cu_2O shells. A search for the structural requirements of the gold cores for the formation of stellated icosahedral Cu_2O nanocrystals identifies icosahedral gold nanocrystals as effective cores for the generation of Au−Cu_2O stellated icosahedra and truncated icosahedra. Trisoctahedral gold nanocrystal cores cannot be used to obtain stellated icosahedra, but they can form face-raised octahedra with V-shaped {111} edges. Remarkably, Au−Cu_2O core−shell cubes and face-raised cubes bounded by essentially {100} facets were inactive toward the photodegradation of methyl orange. On the contrary, face-raised octahedra with more {111} facets showed the best photocatalytic performance. The heterostructures are not only synthetically interesting, but they also reveal important insights into their facet-dependent catalytic properties. Au nanocrystal-enhanced photocatalytic activity is achievable only with proper surface facets of Cu_2O shells.

ASSOCIATED CONTENT

Supporting Information. Schematic illustration of the synthesis procedure, size distribution histograms, XRD patterns, UV−vis absorption spectra, TEM and cross-sectional TEM images, SAED patterns, and SEM images of the heterostructures.

This material is available free of charge via the Internet at http://pubs.acs.org.

AUTHOR INFORMATION

Corresponding Author
*E-mail: hyhuang@mx.nthu.edu.tw.

ACKNOWLEDGMENT

We thank the National Science Council of Taiwan for the support of this research (Grant NSC 98-2113-M-007-005-MY3). The edge- and corner-truncated octahedral gold nanocrystals were synthesized using a method developed by Pei-Ju Chung in our laboratory. We thank Chih-Wen Yang for drawing models of the heterostructures.

REFERENCES

(1) (a) Carbone, L.; Cozzoli, P. D. *Nano Today* **2010**, *5*, 449–493. (b) Casavola, M.; Buonsanti, R.; Caputo, G.; Cozzoli, P. D. *Eur. J. Inorg. Chem.* **2008**, 837–854.
(2) Smith, A. M.; Mohs, A. M.; Nie, S. *Nat. Nanotechnol.* **2009**, *4*, 56–63.
(3) Klimov, V. I.; Ivanov, S. A.; Nanda, J.; Achermann, M.; Bezel, I.; McGuire, J. A.; Piryatinski, A. *Nature* **2007**, *447*, 441–446.
(4) (a) An, K.; Hyeon, T. *Nano Today* **2009**, *4*, 359–373. (b) Zhang, Q.; Wang, W.; Goebl, J.; Yin, Y. *Nano Today* **2009**, *4*, 494–507.
(5) Tsuji, M.; Matsuo, R.; Jiang, P.; Miyamae, N.; Ueyama, D.; Nishio, M.; Hikino, S.; Kumagae, H.; Kamarudin, K. S. N.; Tang, X.-L. *Cryst. Growth Des.* **2008**, *8*, 2528–2536.
(6) Habas, S. E.; Lee, H.; Radmilovic, V.; Somojai, G. A.; Yang, P. *Nat. Mater.* **2007**, *6*, 692–697.
(7) Fan, F.-R.; Liu, D.-Y.; Wu, Y.-F.; Duan, S.; Xie, Z.-X.; Jiang, Z.-Y.; Tian, Z.-Q. *J. Am. Chem. Soc.* **2008**, *130*, 6949–6951.
(8) Lee, Y. W.; Kim, M.; Kim, Z. H.; Han, S. W. *J. Am. Chem. Soc.* **2009**, *131*, 17036–17037.
(9) Lu, C.-L.; Prasad, K. S.; Ho, J.-a. A.; Huang, M. H. *J. Am. Chem. Soc.* **2010**, *132*, 14546–14553.
(10) Wang, F.; Sun, L.-D.; Feng, W.; Chen, H.; Yeung, M. H.; Wang, J.; Yan, C.-H. *Small* **2010**, *6*, 2566–2575.
(11) Yu, Y.; Zhang, Q.; Liu, B.; Lee, J. Y. *J. Am. Chem. Soc.* **2010**, *132*, 18258–18265.
(12) Kuo, C.-H.; Huang, M. H. *J. Phys. Chem. C* **2008**, *112*, 18355–18360.
(13) Ho, J.-Y.; Huang, M. H. *J. Phys. Chem. C* **2009**, *113*, 14159–14164.
(14) Kuo, C.-H.; Huang, M. H. *Nano Today* **2010**, *5*, 106–116.
(15) Kuo, C.-H.; Huang, M. H. *J. Am. Chem. Soc.* **2008**, *130*, 12815–12820.
(16) Kuo, C.-H.; Hua, T.-E.; Huang, M. H. *J. Am. Chem. Soc.* **2009**, *131*, 17871–17878.
(17) Kuo, C.-H.; Yang, Y.-C.; Gwo., S.; Huang, M. H. *J. Am. Chem. Soc.* **2011**, *133*, 1052–1057.
(18) Kuo, C.-H.; Chu, Y.-T.; Song, Y.-F.; Huang, M. H. *Adv. Funct. Mater.* **2011**, *21*, 792–797.
(19) Wu, H.-L.; Kuo, C.-H.; Huang, M. H. *Langmuir* **2010**, *26*, 12307–12313.
(20) Wu, H.-L.; Chen, C.-H.; Huang, M. H. *Chem. Mater.* **2009**, *21*, 110–114.
(21) Ng, C. H. B.; Fan, W. Y. *J. Phys. Chem. B* **2006**, *110*, 20801–20807.
(22) Zhang, Y.; Deng, B.; Zhang, T.; Gao, D.; Xu, A.-W. *J. Phys. Chem. C* **2010**, *114*, 5073–5079.